Brain Struct Funct (2016) 221:2511–2525
DOI 10.1007/s00429-015-1053-4

ORIGINAL ARTICLE

Localization and regulation of PML bodies in the adult mouse brain

Małgorzata H. Hall[1] · Adriana Magalska[1] · Monika Malinowska[1] · Błażej Ruszczycki[1] · Iwona Czaban[1] · Satyam Patel[2] · Magdalena Ambrożek-Latecka[3] · Ewa Zołocińska[1] · Hanna Broszkiewicz[1] · Kamil Parobczak[1] · Rajeevkumar R. Nair[4] · Marcin Rylski[3] · Robert Pawlak[2,5] · Clive R. Bramham[4] · Grzegorz M. Wilczyński[1]

Received: 31 October 2014 / Accepted: 28 April 2015 / Published online: 9 May 2015

Abstract PML is a tumor suppressor protein involved in the pathogenesis of promyelocytic leukemia. In non-neuronal cells, PML is a principal component of characteristic nuclear bodies. In the brain, PML has been implicated in the control of embryonic neurogenesis, and in certain physiological and pathological phenomena in the adult brain. Yet, the cellular and subcellular localization of the PML protein in the brain, including its presence in the nuclear bodies, has not been investigated comprehensively. Because the formation of PML bodies appears to be a key aspect in the function of the PML protein, we investigated the presence of these structures and their anatomical distribution, throughout the adult mouse brain. We found that PML is broadly expressed across the gray matter, with the highest levels in the cerebral and cerebellar cortices. In the cerebral cortex PML is present exclusively in neurons, in which it forms well-defined nuclear inclusions containing SUMO-1, SUMO 2/3, but not Daxx. At the ultrastructural level, the appearance of neuronal PML bodies differs from the classic one, i.e., the solitary structure with more or less distinctive capsule. Rather, neuronal PML bodies have the form of small PML protein aggregates located in the close vicinity of chromatin threads. The number, size, and signal intensity of neuronal PML bodies are dynamically influenced by immobilization stress and seizures. Our study indicates that PML bodies are broadly involved in activity-dependent nuclear phenomena in adult neurons.

Keywords Promyelocytic leukemia · PML · Nuclear body · Cell nucleus · Brain · Cerebral cortex · Seizures · Stress

Electronic supplementary material The online version of this article (doi:10.1007/s00429-015-1053-4) contains supplementary material, which is available to authorized users.

✉ Grzegorz M. Wilczyński
g.wilczynski@nencki.gov.pl

[1] Laboratory of Molecular and Systemic Neuromorphology, Department of Neurophysiology, Nencki Institute of Experimental Biology, Pasteura 3, 02-093 Warsaw, Poland

[2] Department of Cell Physiology and Pharmacology, University of Leicester, University Road, Leicester LE1 7RH, UK

[3] Department of Clinical Cytology, Center of Postgraduate Medical Education, Marymoncka 99/103, 01-813 Warsaw, Poland

[4] Neuroscience Research Group, Department of Biomedicine and KG Jebsen Centre for Research on Neuropsychiatric Disorders, University of Bergen, Jonas Lies vei 91, 5009 Bergen, Norway

[5] Present Address: Hatherley Laboratories, University of Exeter Medical School, Prince of Wales Road, Exeter EX4 4PS, UK

Introduction

The PML protein was first described in the context of its involvement in the pathogenesis of promyelocytic leukemia, from which the protein derives its name; this type of leukemia is caused, in the vast majority of cases, by a specific chromosomal translocation (15; 17), resulting in the disruption of the PML gene, and the expression of an oncogenic fusion protein PML/retinoic acid receptor alpha (RARA) (Warrell et al. 1993). However, later, the expression of PML was described in multiple healthy tissues, i.e., hematopoietic cells, liver and pancreas, gastrointestinal tract, respiratory system, skin, and connective tissues (Gambacorta et al. 1996).

The PML protein appears on the crossroads of multiple signaling pathways and is implicated in a wide range of functions in non-neuronal cells (Bernardi and Pandolfi 2007; Lallemand-Breitenbach and de The 2010), but the role of PML in the nervous system has not been widely investigated. Regad et al. (2009) demonstrated that the physiological function of PML is the maintenance of the neural stem and progenitor cells during the development of the nervous system, and that the expression of PML diminishes after birth. However, recent reports have assigned functions to PML protein in the adult brain (Villagra et al. 2006; Salomoni and Betts-Henderson 2011; Miki et al. 2012, Butler et al. 2013). In the suprachiasmatic nucleus, the PML protein is implicated in the transcriptional regulation of the circadian rhythm (Miki et al. 2012). Expression of PML has also been reported in supraoptic neurons of the normal adult human brain (Villagra et al. 2006). In PML knockout mice, Butler and coworkers described abnormalities in hippocampal long-term potentiation (LTP) and deficits in learning and memory (Butler et al. 2013). There have been also some reports on the involvement of PML protein in the pathogenesis of age-related neurodegenerative disorders (Kumada et al. 2002; Janer et al. 2006; Woulfe et al. 2007). Although the evidence is growing, there is still no cohesive view on the function of PML in the adult brain. One possibility is that PML protein has multiple roles, which vary between brain regions or physiological context. However, because of the lack of comprehensive data on the PML localization among the brain structures, the generalized view on PML functions is not yet available.

The subcellular localization of PML in adult mammalian brain tissue is also little characterized. In non-neuronal cells, the PML protein forms characteristic round-shaped intranuclear inclusions called the PML bodies (Bernardi and Pandolfi 2007; Lallemand-Breitenbach and de The 2010). At the electron microscopic level, typical PML bodies are round structures (0.1–1 μm in diameter) composed of an outer electron-dense fibrillar capsule enveloping the core of variable electron density and composition (Koken et al. 1994). They have been detected in virtually all cell types. Although there is no single cellular function that can be ascribed to the PML bodies, their principal roles at the molecular level are thought to include (a) regulation of transcription and chromatin conformation, (b) sequestration and/or storage of nuclear proteins, (c) degradation of nuclear proteins, and (d) protein post-translational modifications (Lallemand-Breitenbach and de The 2010). The aforementioned biochemical functions translate into the involvement in a variety of physiological process, e.g., antiviral response, apoptosis, cellular senescence, stem cell maintenance, as well as the involvement in pathological phenomena such as tumorigenesis (Bernardi and Pandolfi 2007; Lallemand-Breitenbach and de The 2010).

Because the formation of PML bodies appears to be a key aspect in the function of the PML protein, we investigated the presence of these structures and their anatomical distribution, throughout the adult mouse brain. We also studied their ultrastructure and colocalization with the well-known PML-binding proteins SUMO-1, SUMO 2/3, and Daxx. Finally, we asked whether the neuronal activity has an impact on the form and the intranuclear distribution of PML bodies in neurons. Our study reveals new information on the localization and function of the PML bodies and PML proteins in the brain.

Materials and methods

Subjects

The experiments were performed on 2–3 months old male C57BL6 mice obtained from the Nencki Institute Animal House or from the Animal House of the University of Leicester. The animals were kept under natural light/dark cycle in Plexiglass cages, in a room thermostatically maintained at 22 ± 1 °C, with water and food provided ad libitum. The rules established by the Ethical Committee on Animal Research of Nencki Institute and of the Ethical Committee on Animal Research of University of Leicester were followed strictly in all experiments.

Pentylenetetrazole

In order to stimulate the brain pharmacologically, 2–3 months old C57BL6 mice were injected intraperitoneally with pentylenetetrazole (Sigma Aldrich, cat. No. P6500), 50 mg/kg body weight diluted in saline. Animals were then sacrificed 2 h after the seizure onset.

Immobilization stress

2–3 months old C57BL6 mice were restrained for 6 h in wire mesh restrainers closed on both ends with the clips [as described in (Pawlak et al. 2005)]. After the session, mice were sacrificed.

Histology

Mice were lethally anesthetized with sodium pentobarbital (Biowet Pulawy) in a dose of 100 mg/kg body weight, diluted in saline, and perfused immediately with 0.1 M phosphate-buffered saline (PBS) (pH 7.4), followed by cold 4 % paraformaldehyde (Sigma Aldrich, cat. No. P6148), in PBS (pH 7.4). The brains were cautiously

removed from the skulls and placed for 24 h in the same fixative at 4 °C. Then the brains were cryoprotected with 30 % solution of sucrose in PBS, frozen in the −80 °C cold n-heptane, and stored at −80 °C. Forty-micrometer-thick free-floating sections were cut coronally at −20 °C with the use of the cryostat and stored in anti-freeze solution (30 % glycerol; 30 % ethylene glycol; 0.03 M NaH_2PO_4; 0.01 M NaOH; distilled water), preventing the formation of freezing artifacts.

3,3′-Diaminobenzidine immunohistochemistry

Brains sections from five individuals (24 brain sections from each brain) were washed in PBS (pH 7.4) containing 0.3 Triton X-100 (PBST), then incubated for 30 min in 1 % sodium borohydride (Sigma Aldrich, cat. No. 45, 288-2) in PBS (pH 7.4). The sections were then treated with hydrogen peroxide solution (3 % hydrogen peroxide, 50 % methanol, in distilled water), blocked with 5 % normal horse serum (NHS) (Jackson Immunoresearch, cat. No. 008-000-001) in PBST (pH 7.4), and incubated overnight at 4 °C with the primary antibody (mouse anti-PML antibody, Millipore, cat. No. 05-718, 1:500) diluted in 5 % NHS in PBST. Sections were then washed several times in PBST, and incubated for 1 h at room temperature with biotinylated horse anti-mouse antibody (Vector, BA-2001) diluted 1:200 in 2 % NHS in PBST, followed by a mixture of avidin and biotinylated peroxidase from ABC kit (Vector Laboratories, cat. No. PK-4000). Both of the ABC kit ingredients were diluted 1:400 in PBST. The immunoreaction was developed using 1:1 mixture of 0.1 % of 3,3′-diaminobenzidine tetrahydrochloride (Sigma Aldrich, cat. No. D5637) solution in Tris-buffered saline (pH 7.4) (TBS) and 0.4 % of nickel ammonium sulfate (Sigma Aldrich, cat. No. 574988) dissolved in TBS. After 10 min, H_2O_2 was added to the mixture to a final concentration of 0.003 %. The sections were dried overnight, and then mounted in the DPX medium (Serva, cat. No. 18243.02). As a control for immunoreaction specificity, the tissue samples were stained using non-immune mouse IgG1 (Sigma Aldrich, cat. No. 15381) or NHS (Jackson ImmunoResearch) instead of the primary antibody.

Cell culture

Immortalized mouse fibroblasts (a generous gift from Tomasz Prószyński) were cultured in DMEM culture medium containing 10 % fetal bovine serum, with penicillin and streptomycin, and split every 2 days. For immunofluorescence staining, cells were planted on glass coverslips at the density of 2×10^4 cells/1 cm^2 and after overnight culture, were washed with PBS and fixed with 4 % paraformaldehyde. For electron microscopy, cells were planted on 60 cm^2 petri dishes at the density of 1×10^4 cells/1 cm^2 and grown to a 90 % confluence.

Immunofluorescence

The brain sections (from nine control individuals, five individuals from experimental group: 0.5 h PTZ, six individuals from experimental group: 1 h PTZ, five individuals from experimental group: 2 h PTZ, and eight individuals from experimental group: stress) were incubated in 5 % NHS with 0.1 % Triton X-100 in PBS (pH 7.4) for 1 h. Sections were then incubated in primary antibodies [anti-PML, Millipore, mouse antibody, cat. No. 05-718, 1:200; anti-NeuN, Millipore, chicken antibody, cat. No. ABN91, 1:400; anti-GFAP, Abcam, rabbit antibody, cat. No. AB7260, 1:500; anti-Iba1, Wako, rabbit antibody, cat. No. 019-19741, 1:1000; anti-Olig2, Millipore, rabbit antibody, cat. No. AB9610, 1:500; anti- lamin B (C-20), Santa Cruz Biotech., goat antibody, cat. No. sc-6216, 1:250; anti-Daxx, Santa Cruz Biotech., rabbit antibody, cat. No. sc7152, 1:100; anti-SUMO1 (FL-101), Santa Cruz Biotech., rabbit antibody, cat. No. sc-9060, 1:200; anti-SUMO2/3, Santa Cruz Biotech., rabbit antibody, cat. No. sc-32873, 1:200] overnight at 4 °C in 5 % NHS in PBST solution. After washing, the sections were incubated with secondary antibodies diluted 1:200 in 5 % NHS in PBST solution as follows: (1) in case of the mouse primary antibody, donkey anti-mouse antibody conjugated to DyLight 488 was used (Jackson Immunoresearch, cat. No. 715-546-150), (2) in case of the rabbit primary antibody, donkey anti-rabbit antibody conjugated to Cy3 was used (Jackson Immunoresearch, cat. No. 711-166-152), (3) in case of the chicken primary antibody, donkey anti-chicken antibody conjugated to DyLight 549 was used (Jackson Immunoresearch, cat. No. 703-506-55), (4) in case of the goat primary antibody, donkey anti-goat antibody conjugated to Cy3 was used (Jackson Immunoresearch, cat. No. 705-165-147). The incubation in secondary antibodies lasted for 2 h at room temperature, and the nuclei were stained with the use of near-infrared dye TOPRO3 (Invitrogen, cat. No. T3605) or Hoechst 33342 (Invitrogen, cat. No. H3570). The sections were mounted on microscopic glass slides using Vectashield medium (Vector Laboratories, cat. No. H-1000). The control procedures were performed as described above using non-immune mouse IgG1 (Sigma Aldrich, cat. No. 15381).

Image acquisition and analysis

Chromogenic immunoreactions were recorded using Nikon Labophot microscope equipped with a motorized stage and Image Pro Plus software. Fluorescence microscopy data were collected with the use of the laser

scanning confocal microscope (Zeiss 780), equipped with the Plan-Apochromat 63x/1.4 Oil immersion objective and the following lasers: Diode laser 405 nm (CW/pulsed), Argon lasers (488 and 514 nm), HeNe laser 633 nm. The images were acquired at a pixel count 1024 × 1024. Series of z-stacks were acquired with a step of 0.21 µm. The sampling density of the obtained images was 0.08 µm per pixel. Afterward, deconvolution was performed with the use of the Huygens software (Scientific Volume Imaging). The quantitative three-dimensional analysis of the following parameters: the number, the size, and the fluorescence signal intensity of the PML nuclear bodies were performed using a custom-written segmentation and image analysis software *Segmentation magick* (patent No. EP2549433 A1). The object-based quantitative analysis of colocalization between PML and SUMO-1, and PML and SUMO 2/3 was performed using the Fiji (http://fiji.sc/Fiji) plugin Jacop (http://rsb.info.nih.gov/ij/plugins/track/jacop.html) (Bolte and Cordelieres 2006). The objects within a stack were considered colocalized if the distance between their centers of fluorescence was smaller than the resolution limit of the microscope, which for Zeiss 780 is 220 nm. The material prepared for the electron microscopy was analyzed with the use of the High Performance Biology Transmission electron microscope JEM 1400 (JEOL Co., Japan, 2008) equipped with high-resolution digital camera (CCD MORADA, SiS-Olympus, Germany).

Electron microscopy: immunogold

The procedure was performed according to Wilczynski et al. (2008). Briefly, the perfused brains (from three individuals from the control group) were cut with the use of a vibratome (Leica, VT1000 S) into 200 µm-thick sections, which were subsequently placed in 30 % sucrose for cryoprotection. The immortalized fibroblasts were fixed with 4 % paraformaldehyde in PBS, washed with PBS, scrubbed from the dish, and centrifuged with 500×*g* for 5 min. The supernatant was discharged and the pellet was placed in 4 % sucrose. Both types of samples were then high-pressure frozen using EM PACT system (Leica). In order to optimally preserve both, the antigenicity and ultrastructure, the frozen samples were subjected to osmium-free freeze substitution followed by Lowicryl HM20 (Polysciences, Inc., cat. No. 23994-225) embedding, and UV-induced polymerization at −50 °C, using EM ASF2 apparatus (Leica). Ultrathin sections were cut in an ultramicrotome (Leica Ultracut R; Leica), and mounted on 300 mesh nickel grids coated with formvar (Agar Sciences, cat. No. S138N3). The sections placed on grids were immersed in 50 mM glycine in Tris-buffered saline supplemented with 0.1 % Triton X-100 (TBST) for 10 min. Later samples were blocked in TBST containing 2 % bovine serum albumin (BSA) (Sigma Aldrich, cat. No. A7030) for 10 min, and then incubated in the primary antibody (1:50, PML, Millipore) overnight at room temperature. After washing in TBST (first three times short by immersing each grid in TBST by a fast movement, then followed by a long wash in a TBST drop, for 10 min) samples were incubated in secondary antibody coupled to 10 nm colloidal gold particles diluted 1:20 (Donkey anti-Mouse IgG (H&L) EM-grade 10 nm, Electron Microscopy Sciences, cat. No. 25815) in 2 % BSA and 0.005 % polyethylene glycol (PEG 2000, Merck, cat. No. A07062) for 1 h, rinsed with distilled water, incubated in 4 % uranyl acetate in water for 15 min, washed with distilled water, and left for drying.

Statistical analysis

The cumulative distributions of the parameters describing the characteristics of PML nuclear bodies (number of bodies per nucleus, body size, and fluorescence intensity) were compared using Kolmogorov–Smirnov test. The cumulative distribution for the control group was quantitatively compared with the cumulative distribution for the stress/pentylenetetrazole groups. For the cases when the Kolmogorov–Smirnov test revealed a statistical significance (p value <0.001), further post hoc analysis was performed, in order to identify the details by which the distributions differ from each other. The randomization test (1000 resamplings) was performed to test the differences between the distributions against the null hypothesis. After binning the data, we recorded the bins for which the difference between the distributions (or a larger one) could not be obtained with 99.73 % probability (p value <0.003). For the qRT-PCR, the medians and quartiles of three individuals, each analyzed in four replicates, are shown. Bootstrap test (Cleries et al. 2012) showed no statistical significant difference between each condition and the control (p value for PTZ seizures <0.2005, p value for stress <0.183).

Western blotting

The cortices, from three individuals per treatment, were dissected in less than 1 min after removal of the brains from the skulls, and nuclear extracts were obtained using ProteoExtract Subcellular Proteome Extraction Kit (Millipore, cat. No. 539790). Samples were subjected to SDS/PAGE electrophoresis and transferred onto nitrocellulose membrane. After blocking in 5 % skim milk, 0.1 % Tween 20 in PBS for 1 h at room temperature, the membranes were probed with mouse anti-PML antibody, [(PML-97) Abcam, cat. No. ab50637, 1:750 in blocking solution, at 4 °C, overnight] followed by an anti-mouse peroxidase-

conjugated secondary antibody (Amersham Biosciences, cat. No. NA931vs, 1:10000 in blocking solution, 1 h at room temperature), and the signal was developed using ECL Prime kit GE (Healthcare, Amersham, cat. No. RPN 2232). The results were normalized to nuclear protein Matrin-3 (Abcam, cat. No. Ab151714, 1:5000).

Quantitative RT-PCR

Total RNA was extracted from cortices isolated immediately after removal of the brains from three individuals per each treatment, using RNeasy Mini Kit (Qiagen, 74104) according to manufacturer's instructions. The 1 μg of total RNA was used in reverse transcription reaction with 10 μM deoxynucleotide triphosphates (Fermentas, R0192), 1.25 μM oligo $d(T)_{16}$primer (Invitrogen, N8080128), 1.25 μM of random hexamers (Invitrogen, N8080127), 20 units of RiboLock RNase inhibitor (Thermo Scientific, EO0381), and 100 units of SuperScript III Reverse Transcriptase (Invitrogen, 18080–044) in total volume of 20 μl. The cDNA synthesis was achieved by incubation at 25 °C for 5 min followed by incubation at 50 °C for 60 min. The qPCR reactions were performed with 1 μl of cDNA and specific primers (0.2 μM) for PML: forward-CCGAAGA CTATGAACACAGCCA, and reverse-CAGCAGTTTG GGGCACTTG, resulting in 110 bp product; and for control gene GAPDH: forward-TGACCTCAACTACATGG TCTACA, reverse-CTTCCCATTCTCGGCCTTG, resulting in 85 bp product, which was used for normalization. The primers were designed with Primer3 software (Koressaar and Remm 2007; Untergasser et al. 2012). The qRT-PCR reactions and fluorescence measurements were performed using a SYBR® Green Real-Time PCR Master Mix, LightCycler ABI7300 Real-Time PCR system (Applied Biosystems), and the following parameters; the initial denaturation at 95 °C for 10 min, followed by 40 cycles of denaturation at 95 °C for 30 s, annealing at 60 °C for 30 s, and elongation at 72 °C for 30 s. All sample analyses were performed in quadruplicates. The relative expression of PML in each treatment was calculated according to the guidelines of Real-Time PCR handbook: http://www.uic.edu/depts/rrc/cgf/realtime/data.html.

Results

PML protein expression pattern in adult mouse brain

In order to determine the expression of the PML protein throughout the brain we performed immunohistochemistry with the use of anti-PML antibody, the specificity of which was confirmed in PML knockout animals (Regad et al. 2009). In general, the expression of PML was confined to the gray matter. In the coronal brain sections, the PML immunostaining varied considerably between brain regions (Fig. 1). In the telencephalon, PML was most abundantly expressed in the neocortex and basal ganglia. The PML immunoreactivity in diencephalon was weak overall, with the exception of the medial habenular nucleus, and several thalamic nuclei. Likewise, the PML expression in mesencephalic and mesencephalic structures was low to medium, with the very prominent exception of cerebellar cortex. The strong signal of the fimbria hippocampi was unspecific as found using non-immune IgG labeling (Suppl. Figure 1). The detailed semi-quantitative description of PML presence across brain regions is presented in the Table 1.

To characterize PML distribution at the cellular level, we focused on somatosensory cerebral cortex, in which the strongest staining was observed in the upper layers, especially in the layer IV (Fig. 2a). In neurons, PML immunoreactivity (IR) formed numerous distinctive roundish nuclear bodies, with diameters 0.2–0.5 μm (Fig. 2b–d). However, in imaging conditions, which caused nuclear signal to become oversaturated some amount of specific immunoreactivity could be observed also in the nucleoplasm, (Suppl. Figure 2). The cytoplasmic PML immunoreactivity was low in the cortical neurons, yet it could be observed therein under the conditions of oversaturation (Suppl. Figure 2). In addition, in some brain areas, such as hippocampus and striatum, there was stronger extranuclear staining (Suppl. Figure 2). Among cortical neuronal subpopulations only excitatory, but not inhibitory neurons expressed this protein (Fig. 2e–g). To determine whether the PML protein is present in other cell types, we performed co-immunostaining for PML and markers of microglia (Fig. 3a–c), oligodendrocytes (Fig. 3d–f), and astrocytes (Fig. 3g–i). We found that PML-IR is essentially absent from all these cell types.

PML body structure and composition in cortical neurons

Next we investigated the fine structure of PML bodies in neuronal nuclei. As the highest resolution tool for this purpose we used electron microscopy and immunogold staining to analyze neurons of layer IV of the mouse cerebral cortex. We chose staining of fibroblasts as a comparison for the results obtained in neurons, as the expression of the PML protein in this type of cells is already well documented (Zhong et al. 2000). The electron micrographs of fibroblasts reveal the PML bodies as distinct clusters of colloidal gold particles overlying the round areas of somewhat increased electron density (Fig. 4a). In contrast, in layer IV cortical neurons, the PML protein

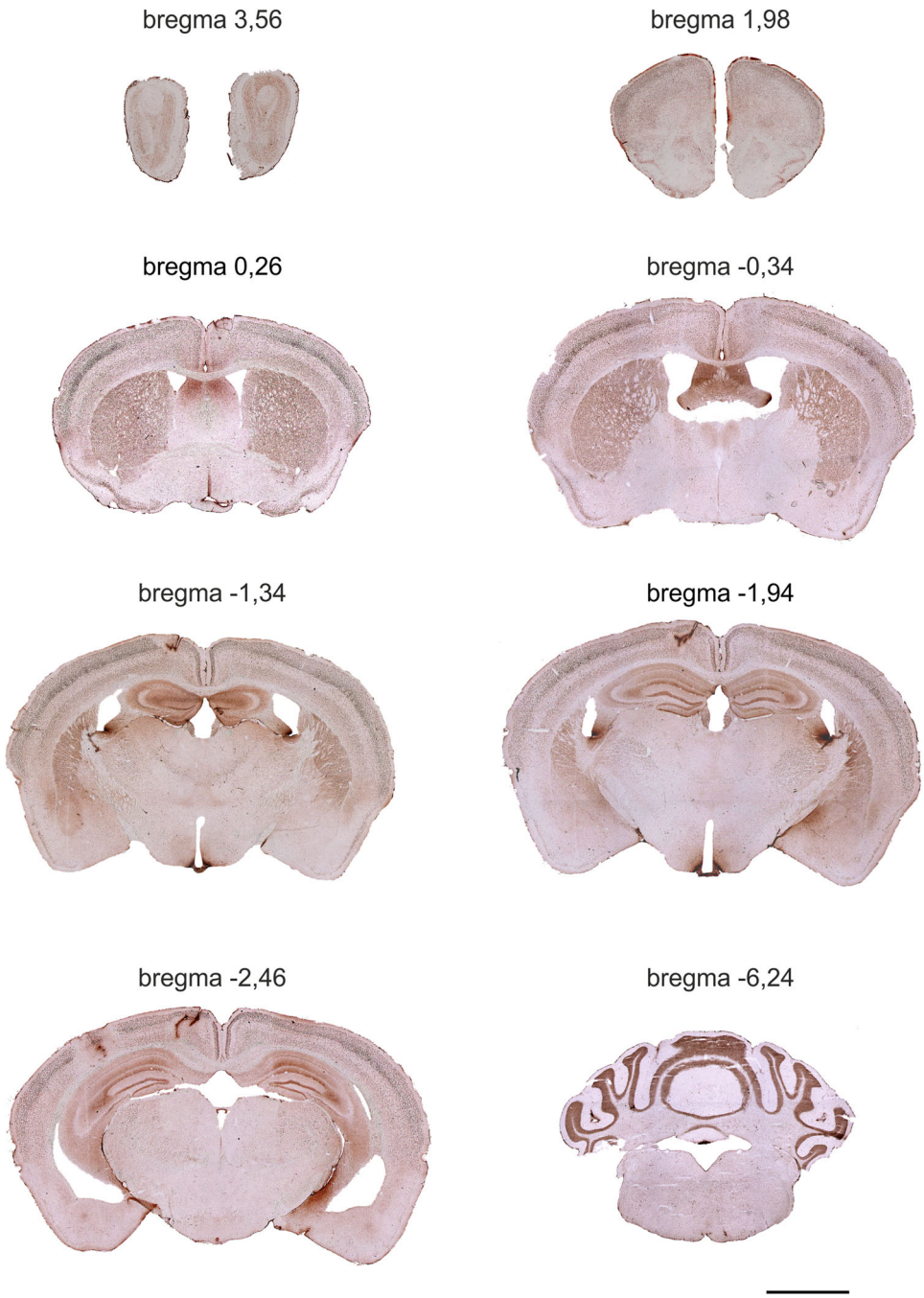

Fig. 1 PML protein expression throughout the brain. Consecutive coronal sections of the rat brain in which PML was visualized using DAB immunohistochemistry. Note the dominant expression in the cerebral and cerebellar cortices, as well as variable expression within other areas. The positions of the given sections along the sagittal axis is indicated above the section as the distance from the bregma. The *scale bar* 1 mm

forms small aggregates scattered throughout the nucleoplasm in close apposition to the thin chromatin fibrils (Fig. 4b). To determine whether the protein composition of the neuronal PML bodies is different from that of fibroblasts, we analyzed whether they contained typical PML body resident proteins: SUMO-1, SUMO-2/3, and DAXX. We found that 18.1 ± 2.2 % neuronal PML bodies colocalize with the immunoreactivity of SUMO-1 (Fig. 4 f–h). The size of PML immunoreactive structures did not correlate with the presence or absence of colocalization with SUMO-1. (0.251 vs. 0.243 µm, respectively for the PLM bodies containing SUMO-1, and those that did not contain SUMO-1). The colocalization was much lower in case of SUMO-2/3 (2.8 ± 1.1 %) (Suppl. Figure 3, Suppl. Figure 4). Notably, in contrast to fibroblast PML bodies that colocalize both with SUMO-1 and DAXX, neuronal PML bodies did not exhibit DAXX immunolabeling (Fig. 4 l–n).

Table 1 PML expression throughout the brain

Structure	Level of PML expression	Density of nuclei with PML expression
Prosencephalon		
Telencephalon		
Olfactory bulb		
Layers of the olfactory bulb		
External plexiform (EPI)	+	++
Mitral cell (Mi)	+	+++
Internal plexiform (IPI)	+	+++
Granule cell layer (GrO)	+	+++
Olfactory nerve layer (ON)	0	0
Tenia tecta		
Dorsal tenia tecta (DTT)	+	++
Ventral tenia tecta (VTT)	++	++
Olfactory tubercle (Tu)	+	+++
Cerebral cortex		
Layers		
I	0	0
II	++	++
III	++	++
IV	+++	+++
V, VI	++	++
Structures		
Dorsolateral orbital cortex (DLO)	+++	+++
Frontal association cortex (FrA)	++	+++
Prelimbic cortex (PrL)	++/+++	+++
Medial orbital cortex (MO)	++/+++	+++
Ventral orbital cortex (VO)	+++/++	++
Lateral orbital cortex (LO)	+++/++	++
Cingulate cortex (Cg1)	+++	+++
Cingulate cortex (Cg2)	+++	+++
Motor cortex (M1, M2)	++	++
Frontal cortex (Fr3)	++	++
Insular agranular cortex		
Dorsal part (AID)	+	++
Ventral part (AIV)	+	++
Primary somatosensory		
Cortex (S1)	++	++
Jaw region (S1J)	++	++
Dysgranular zone (S1DZ)	+++	+++
Forelimb region (S1FL)	+++	+++
Upper lip region (S1ULp)	+++	+++
Insular cortex		
Granular (GI)	+/++	++
Dysgranular (DI)	+/++	++
Agranular cortex		
Posterior part (AIP)	+	+
Retrosplenial cortex		
Dysgranular cortex (RSD)	+++	+++
Granular cortex		
a region (RSGa)	+++	+++
b region (RSGb)	+++	+++
c region (RSGc)	+++	+++
Ectorhinal cortex (Ect)	+++	++
Perirhinal cortex (PRh)	+++	++
Association cortex		
Medial parietal (MPtA)	+++	++
Lateral parietal (LPta)	+++	++
Temporal (TeA)	+++	++
Auditory cortex		
Primary auditory cortex (Au1)		
Secondary auditory cortex		
Dorsal area (AuD)	+++	++
Ventral area (AuV)	+++	++
Entorhinal cortex		
Dorsintermed (DIEnt)	+	+
Dorsolateral (DLEnt)	+	+
Ventral intermediate (VIEnt)	+	+
Visual cortex		
Primary cortex (V1)	+	+
Binocular area (V1B)	+	+
Secondary cortex		
Lateral area (V2L)	++	+++
Mediolateral area (V2ML)	++	+++
Mediomedial area (V2MM)	++	+++
Medial entorhinal cortex (MEnt)	0	0
Entorhinal cortex (CEnt)	0	0
Piriform cortex (Pir)	+	+++
Corpus callosum		
Forceps minor of the cc (Fmi)	0	
Genu of the cc (Gcc)	0	
Corpus callosum (cc)	0	
Accumbens nucleus		
Core (AcbC)	++	+++
Shell (AcbSh)	++	+++
Lateral Shell (LAcbSh)	++	+++
Hippocampus		
Field CA3 (CA3)	++	+++
Field CA2 (CA2)	0	0
Field CA1 (CA1)	+	+++
Dentate gyrus (DG)	++	+++
Basal ganglia		

Table 1 continued

Structure	Level of PML expression	Density of nuclei with PML expression
Striatum		
Caudate putamen (CPu)	+++	++
Diencephalon		
Thalamus		
Habenula		
Medial habenular nucleus (MHb)	+++	+++
Lateral habenular nucleus (LHb)	0	0
Thalamic nuclei		
Paratenial nucleus (PT)	++	+
Paraventricular nucleus		
Anterior part (PVA)	0	0
Paraventricular nucleus (PV)	0	0
Ventral posterolateral (VPL)	++	+
Ventral ant nucleus (VA)	0	0
Ventrolateral nucleus (VL)	0	0
Medial (VM)	0	0
Ventral posteromed (VPM)	++	+
Central medial nucleus (CM)	++	+
Paracentral nucleus (PC)	++	+
Centrolateral nucleus (CL)	++	+
Post nuclear group (Po)	0	0
Reuniens (Re)	0	0
Ventral Reuniens (VRe)	0	0
Xiphoid thal nucleus (Xi)	0	0
Med geniculate nucleus		
Dorsal (MGD)	++	++
Medial (MGM)	++	++
Ventral (MGV)	++	++
Hypothalamus		
Septum		
Septohippocampal nucleus (SHi)	+	+
Paraventricular nucleus		
Anterior part (PaAP)	+++	+
Periventricular nucleus (Pe)	0	0
Striohypothalamic nucleus (StHy)	++	+
Arcuate nucleus (Arc)	++	++
Paravent hypothalamus magnocel		
Medial (PaMM)	++	+
Lateral (PaLM)	++	+
Medial parvicellular (PaMP)	++	+
Nucleus vent (PaV)	++	+
Hypothalamic nucleus		
Lateroanterior (LA)	+++	+
Dorsomed (DM)	+	++
Lateral septal nucleus		
Dorsal part (LSD)	0	0
Intermediate part (LSI)	0	0
Medial septal nucleus (MS)	0	0
Preoptic area		
Suprachiasmatic nucleus (SCh)	+	++
Dorsolateral part (SChDL)	+	++
Substantia innominata (SI)	0	0
Nucleus of the vertical limb of the diagonal band (VDB)	0	0
Bed nucleus of the stria terminalis (STM)	+	++
Medial Preoptic nucleus (MPO)	++	++
Mesencephalon	0	0
Medial Mammilliary nucleus (MM)	+	++
Cerebral peduncles tectum		
Superior colliculus (SC)	++	+
Dorsal endopiriform claustrum (DEn)	++	+
Lateral amygdaloid nucleus (La)	++	+
Globus Pallidus (GP)	+	+
Inferior colliculus (CI)	+	+
Dorsomedial spinal trigeminal nucleus (DMSP5)	++	+
Rhombencephalon		
Metencephalon		
Cerebellum		
Cerebellar cortex		
Molecular layer (ML)	0	0
Layer of large purkinje cells	+++	++
Granular layer (GL)	+++	+++
White matter (WM)	0	0
Ventral cochlear nucleus		
Anterior part (VCA)	+	+
Posterior part (VCP)	+	+
Dorsal cochlear nucleus (DC)	++	+
Fusiform layer (DCFu)	++	+
Molecular layer (DCMo)	++	+

Table 1 continued

Structure	Level of PML expression	Density of nuclei with PML expression
Granule cell layer of cochlear nucleus (GrC)	0	0
Pons		
Pontine nuclei (Pn)	+	+
Myelencephalon		
Dorsal motor n of X caudoventral reticular nucleus (CVL)	+	++
Nuclear solitary tract (SOL)	+	++
Spinal trigeminal nucleus (Sp5I)	+	++

Changes in PML body size, number, and fluorescence intensity following seizure activity and immobilization stress

To determine whether PML bodies can be regulated by brain activity, we used two forms of acute stimulation: (1) stress resulting from immobilization for 6 h, and (2) pharmacological stimulation with pentylenetetrazole, a GABA-A receptor antagonist, that causes a brief seizure after intraperitoneal administration. In both cases we performed an extensive analysis of the number, size, and signal intensity of PML bodies in confocal stacks taken from the cortical layer IV, using our proprietary high-throughput automatic segmentation and analysis software "Segmentation magick" (Walczak et al. 2013). The results are presented in Fig. 5 as graphs displaying the probability density of the occurrence of the nuclei with a given value of the measured parameters. After 6 h of immobilization, we observed a prominent increase of the size and fluorescence intensity of the PML nuclear bodies, and a substantial decrease of their number per nucleus. In the experiment with pentylenetetrazole we performed the analyses at 30 min, 1, and 2 h after injection. We found a biphasic behavior of the PML bodies. At 30 min time point there was a decrease in size, but no significant changes in number or fluorescence intensity of the bodies. In contrast, after 1 h the PML bodies were substantially larger and less numerous, compared to control. Concomitantly, the distribution of fluorescence intensity broadened, i.e., there were both very dim and very bright bodies compared to control. The changes further aggravated after 2 h post-injection. Notably, these alterations were not accompanied by changes in expression of the PML mRNA and protein, as determined using quantitative RT-PCR analysis and Western blotting, respectively (Suppl. Figure 5). The morphological transformations of PML bodies upon stimulation were also not associated with the changes of

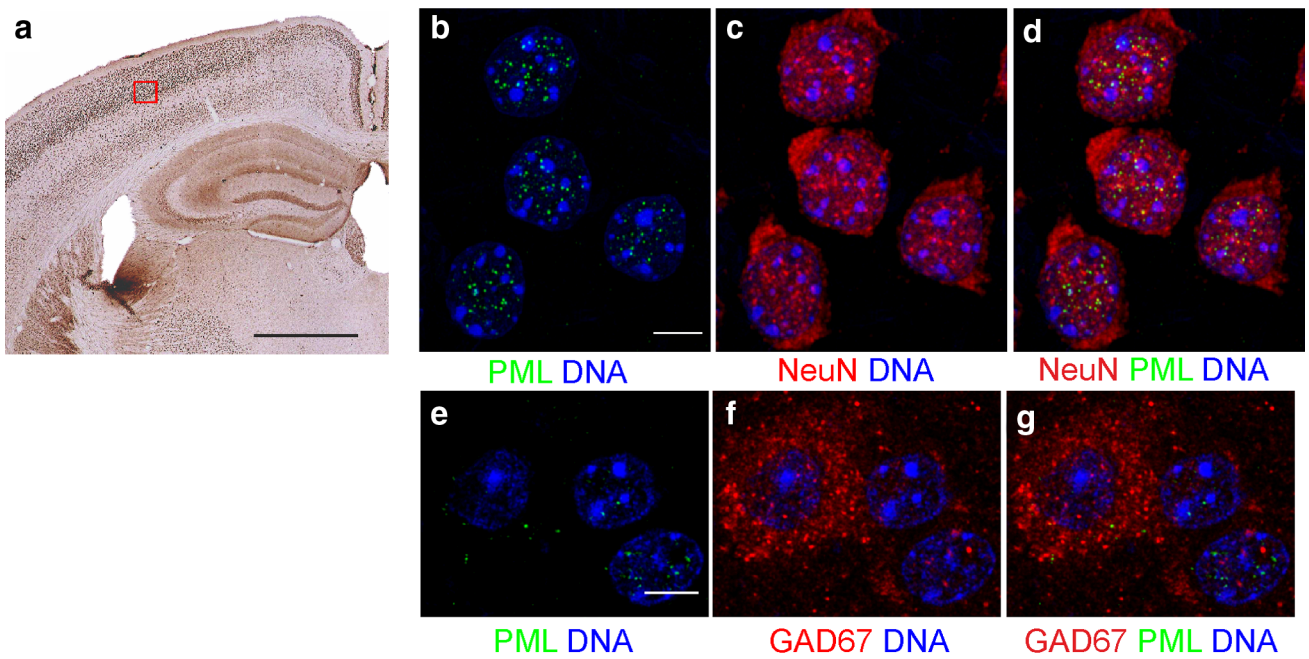

Fig. 2 **a** Enlarged view of the cerebral cortex showing variable PML expression among its different layers (DAB immunohistochemistry). **b–d** Fluorescent confocal images of neurons from cortical layer IV, immunolabeled for PML (*green*) and a neuronal marker NeuN (*red*). Note the distinctive nuclear PML bodies. **e–g** Confocal image of an interneuron expressing GAD67 marker (*red*) that is devoid of PML bodies, in contrast to the neighboring neurons; the image is taken from layer IV. In **b–g** DNA was counterstained using ToPro3 (*blue*); the *scale bars* in **a** −1 mm, in **b–g** −5 μm

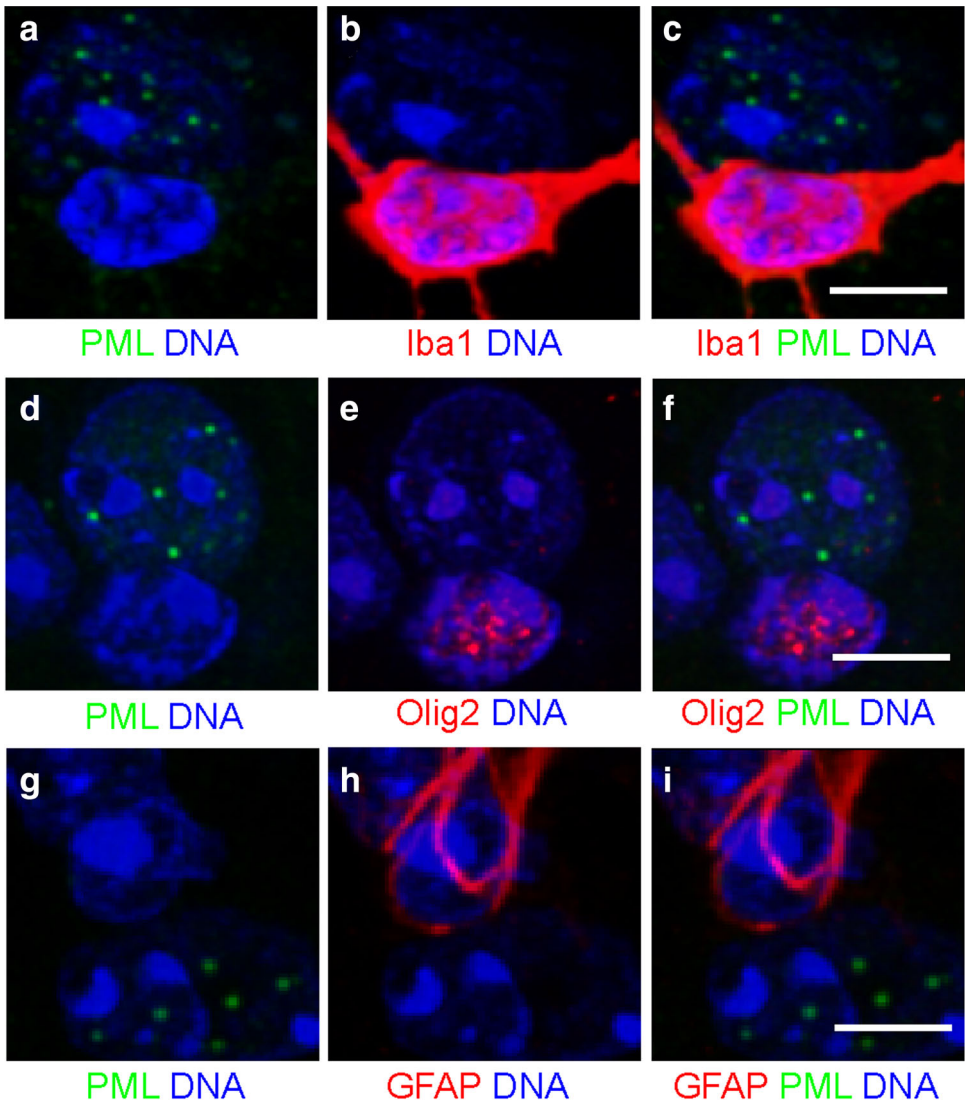

Fig. 3 PML expression in glial cells. The significant expression of the PML protein was not observed in various types of glial cells: microglia (**a**, **b**, **c**), oligodendrocytes (**d**, **e**, **f**) and astrocytes (**g**, **h**, **i**). In contrast, the neighboring neurons contain distinctive PML bodies (*green*). The cells were visualized with the following markers: Iba 1 (microglia), Olig2 (oligodendrocytes), GFAP (astrocytes), all in *red*. DNA was counterstained using ToPro3 (*blue*). The *scale bars* 5 µm

their colocalization with SUMO-1 or SUMO-2/3 (Suppl. Figure 4). Likewise, there was no shift in the molecular weight of PML protein in blots, which would indicate the change in its sumoylation (Suppl. Figure 5).

Discussion

Our study presents the analysis and quantification of the expression, composition, and spatiotemporal arrangement of PML protein and PML nuclear bodies in neurons of the mouse brain. Previously, Regad et al. (2009) demonstrated an important role of the PML protein in the prenatal differentiation of the neural progenitor cells, through the influence of PML on the phosphorylation state of the retinoblastoma protein. The lack of PML affected the transition between radial glial cells and basal progenitor cells, resulting in a decreased thickness of the cerebral cortex in PLM knockout animals. Although the overall expression of the PML protein strongly decreased after birth, a small number of cells in the hippocampus retained the strong PML immunoreactivity at P7. Whether the PML protein plays a role in the postnatal hippocampal neurogenesis, as suggested by Butler et al. (2013), remains an intriguing possibility for further studies.

Although the presence of PML protein in the adult mouse brain has been reported (Miki et al. 2012; Butler et al., 2013), the present work is a comprehensive analysis of PML bodies as distinctive structures in mouse neurons. At the light microscopic level, these bodies have a granular appearance that is similar to that described in the majority of non-neuronal cells. They also closely resemble small PML bodies identified by Villagra et al. (2006) in human supraoptic neurons. However, they are clearly different form large donut-shaped structures observed in some cells, including a subset of supraoptic neurons (Villagra et al.

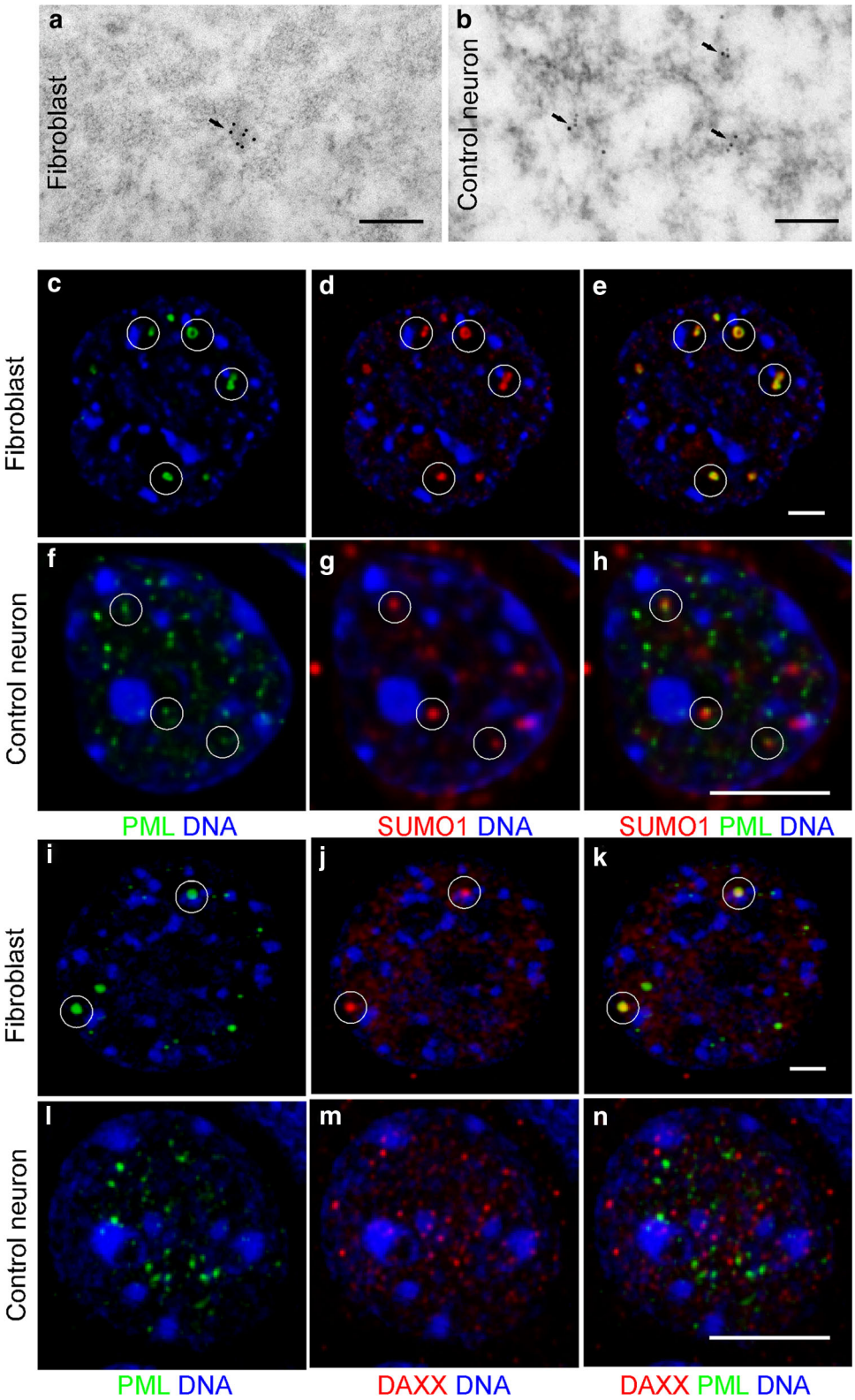

Fig. 4 PML bodies structure and composition. The PML protein, as shown by the electron microscopic immunogold analysis (**a**, **b**), form distinctive PML nuclear bodies in fibroblast nuclei (**a**), in contrast to neuronal nuclei (**b**). The gold particles in the neuronal nuclei display dispersed localization of the PML protein within the nucleoplasm. Most of those small PML aggregates localize in the proximity of the chromatin strands (**b**). On the contrary, fibroblast has distinctive PML nuclear bodies (**a**), positioned within their interchromatin space (**a**). The *scale bars* in each right corner of electron micrographs represent the length of 200 nm. **c**–**n** Confocal images demonstrating the colocalization of PML (*green*) with SUMO-1 (*red* in **c**–**h**), and with DAXX (*red* in **i**–**n**) both in fibroblasts (**c**–**e**, **i**–**k**) and neurons (**f**–**h**, **l**–**n**); Note that PML colocalizes with SUMO-1 in both cell types, but with DAXX only in fibroblasts. DNA was counterstained using Hoechst (*blue*). The *scale bars* 5 μm

2006). At the ultrastructural level, the morphological difference between PML bodies described herein and classic PML bodies, being surrounded by more or less distinctive capsule (Lallemand-Breitenbach and de The 2010), is striking. The lack of peripheral ring (at least in the cerebral cortex) might indicate that the function of PML bodies in

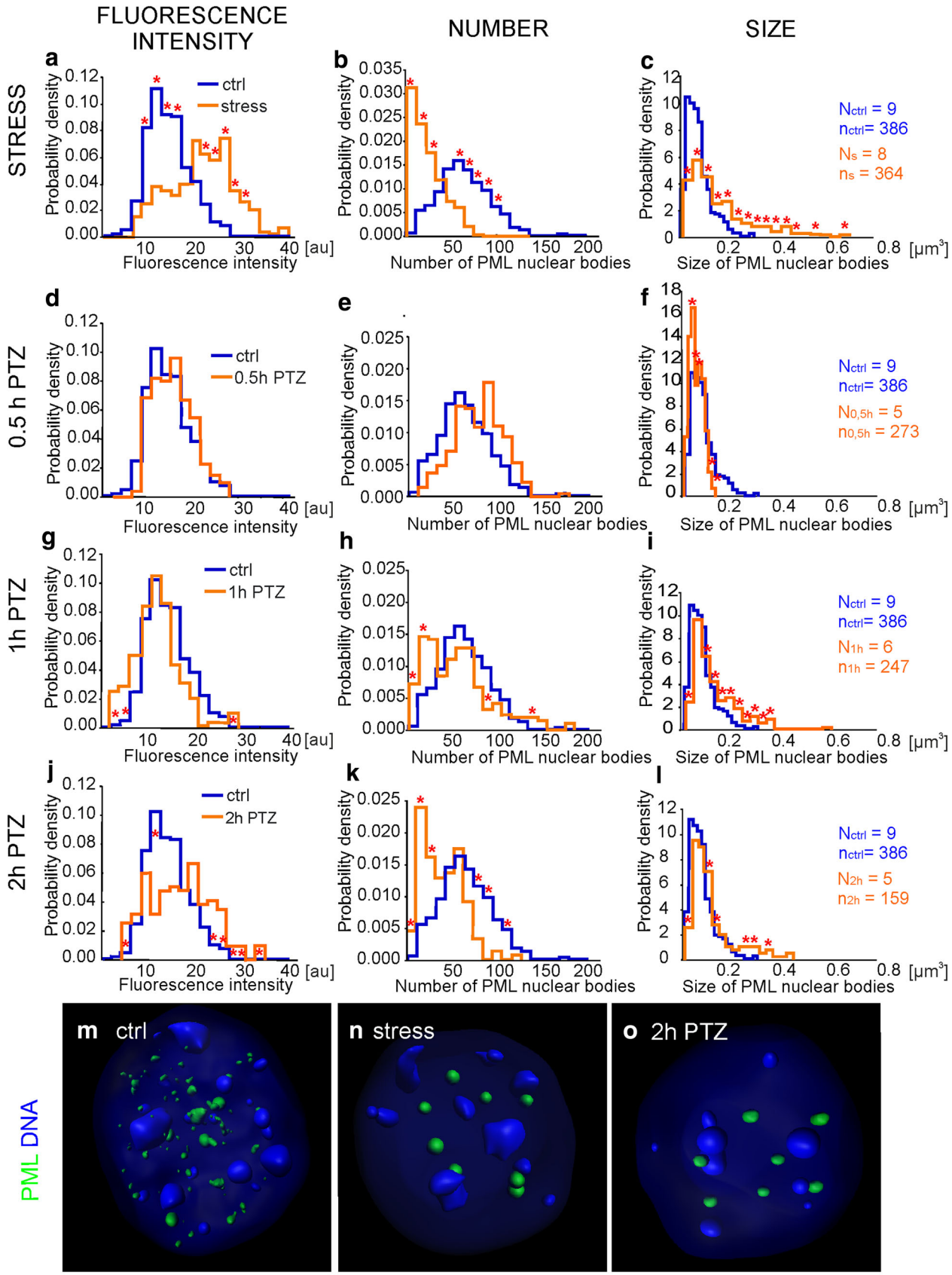
FLUORESCENCE INTENSITY
NUMBER
SIZE
STRESS
0.5 h PTZ
1h PTZ
2h PTZ
a
b
c
d
e
f
g
h
i
j
k
l
ctrl
stress
0.5h PTZ
1h PTZ
2h PTZ
Probability density
Fluorescence intensity
[au]
Number of PML nuclear bodies
Size of PML nuclear bodies
[μm³]
Nctrl = 9
nctrl= 386
Ns = 8
ns = 364
N0,5h = 5
n0,5h = 273
N1h = 6
n1h = 247
N2h = 5
n2h = 159
PML DNA
m ctrl
n stress
o 2h PTZ

◀**Fig. 5** The PML nuclear bodies in stimulated brain. The graphs demonstrate the distributions of the fluorescence intensity (**a**, **d**, **g**, **j**), number (**b**, **e**, **h**, **k**) and size (**c**, **f**, **i**, **l**) of PML bodies in control animals (*blue lines*) and animals subjected to the immobilization stress (**a**–**c**) or pentylenetetrazole treatment (**d**–**l**) (*orange lines*); the analyses were performed at three time points after pentylenetetrazole-induced seizures: 30 min (**d**–**f**), 1 h (**g**–**i**), 2 h (**j**–**l**). In each graph, the *vertical axis* represents the probability density of finding the nucleus with the given values of the respective parameters characterizing PML bodies: fluorescence intensity, number, and size (displayed on the *horizontal axis*). Note that stress increases fluorescence intensity and the size of PML bodies, while it decreases their number. The behavior of PML bodies after pentylenetetrazole depends on the time point. At 30 min time point there was a decrease in size, but no significant changes in number or fluorescence intensity of the bodies. In contrast, after 1 h the PML bodies were substantially larger and less numerous, compared to control. Concomitantly, the distribution of fluorescence intensity broadened, i.e., there were more both, very dim and very bright, bodies compared to control. The changes further aggravated after 2 h post-injection. To better visualize those differences the three-dimensional reconstructions of the representative nuclei from control, stress, and pentylenetetrazole group (2 h) are shown below (**m**, **n**, **o**). *N* represents the total number of animals used, *n* represents the total number of analyzed nuclei

the brain compared to PML bodies in other organs is different. In fact, the PML bodies in cortical neurons resemble the microbodies that are detected in malignant leukocytes of the promyelocytic leukemia patients (Koken et al. 1994). Similar structures appear after DNA damage and some other forms of cellular stress (Eskiw et al. 2003, 2004; Salomoni et al. 2005). The microbodies are thought to represent the PML pool engaged in direct interactions with chromatin, including transcription. In addition, we do not exclude the presence of some amount of PML protein in the diffuse form, as suggested by our confocal experiments performed under oversaturated conditions. Similar to classic PML bodies, the inclusions described by us contain SUMO-1, and, to the lesser extent SUMO-2/3, but they do not contain DAXX. The apparent lack of the colocalization between PML and DAXX is surprising, since the interaction of these proteins and its relevance to chromatin remodeling by H3.3 histone insertion is already well established (Salomoni 2013). It is even more surprising given an important role of DAXX in the activity-dependent H3.3 insertion in neurons (Michod et al. 2012). Our study suggests that PML involvement in neuronal activation is separate from the PML-SUMO-DAXX pathway. The consequences of such situation are, presently, unknown. The difference between PML body colocalization with SUMO-1 and with SUMO-2/3 could be potentially important, since particular SUMO family members are known to behave differently in various physiological and pathological conditions (Guo and Henley 2014; Guzzo et al. 2014). For example, SUMO-1 was shown to promote cell death (Guo et al. 2013), while SUMO-2/3 were shown to be cytoprotective (Wasiak et al. 2007). The actual binding of SUMO-1 and SUMO 2/3 to PML protein should be investigated by immunoprecipitation. The relationship of neuronal PML bodies, described by us, to clastosomes discovered by Lafarga et al. (2002) remains to be determined.

Our study is the first to report the regulation of PML body size, number, and signal intensity, which reflects the PML concentration, by brain stimulation. It seems that the common feature of the two models that we used, resulting ultimately in very similar appearance of PML bodies, is strong neuronal activation. Indeed, the massive sensory stimulation occurs as the animal tries to free itself from the wire mesh during restrain experiments. Our time-course analysis after seizure revealed a dynamics of activity-dependent remodeling of the PML bodies. We speculate that initial dispersion of the bodies, evident 30 min after PTZ, results from their fission, and is followed by their coalescence into less numerous larger structures at the later time points. The increase in number of bodies at 30 min time point is not accompanied by the decrease in body size likely because after fission the resulting structures fall below the resolution limit, so their true volume cannot be estimated correctly. The fusion–fission scenario is supported by the absence of changes in PML expression, as revealed by qRT-PCR and Western blotting. The phenomenon resembles to some extent the early steps after treatment of cells with arsenic (Zhu et al. 1997), however the sequence of events appears not to evolve in this case to PML hyper-sumoylation and degradation. The absence of increased sumoylation is consistent with the results of the PML-SUMO-1 and PML-SUMO-2/3 colocalization analysis and with the apparent lack of changes of PML molecular weight by Western blotting. Since the binding of SUMO is a crucial event in PML aggregation, it is unclear how it occurs in neurons. However, most recent study demonstrated that PML aggregation and nuclear body formation may be independent of PML sumoylation (Sahin et al. 2014).

The distinct ultrastructural form of PML bodies in neurons, and their close proximity to chromatin fibrils, suggests their involvement in gene expression phenomena. Indeed the role of PML in transcription, including its direct binding to transcription factors such as serum response factor (SRF) and c-Fos, has been described (Vallian et al. 1998; Matsuzaki et al. 2003). In fact, both aforementioned factors are involved in the neuronal activity-dependent gene expression (Okuno 2011). The prominent change in PML body distribution found by us 2 h after pentylenetetrazole-induced seizure is coincident with the peak of expression of proteins encoded by immediate-early genes, as reported in the literature. Therefore, our results are harmonious with the work by Butler et al. (2013) that demonstrated cognitive deficiencies in PML knockout

animals. However, in order to rule out the possibility that these deficiencies result from disturbed brain development in utero, one would need a conditional knockout.

Our detailed morphological study on the distribution of the PML bodies in the adult brain is largely consistent with the results obtained by Butler et al. (2013) who used Western blotting to determine the relative abundance of PML protein in the cortex, hippocampus, cerebellum, and brain stem. There is, however, a difference with regards to the hippocampus, which was reported to contain essentially the same amount of PML protein as the cortex. In our study, the signal intensity and the number of PML bodies in all hippocampal layers are much less than the corresponding values in the cortex. We suggest that this discrepancy can be explained by the presence of diffuse staining in the neuropil of the hippocampus in our study, which most probably represent the cytoplasmic PML pool that contributed to the overall amount of the protein in this structure. The existence of cytoplasmic PML could explain the deficiency of hippocampal early phase LTP, which does not depend on gene expression phenomena (Butler et al. 2013). The disturbed E-LTP could be consistent with the reported function of cytoplasmic PML protein in calcium homeostasis (Giorgi et al. 2010). However, it is important to note that the antibody that we used to visualize PML distribution detects both rodent PML isoforms (PML I, PML II); it is possible that the different localization of the signal, i.e., nuclear vs. cytoplasmic reflects the presence of different PML isoforms. On the other hand, we confirm the results by Miki et al. (2012), who showed the expression of PML protein in neurons from suprachiasmatic nucleus (SCN), and the involvement of PML in the generation of circadian rhythm therein; relatively weak PML expression in SCN (Table 1), in our study, is probably related to the particular time during the day in which the animals were killed that does not correspond to the peak level of PML expression in that structure.

Another issue that needs to be addressed is the very selective presence of PML body in distinct structures of the brain. For example the PML staining is very strong in the layer IV of the cortex, but very weak in the adjacent pyramidal layer V. There are a few proteins that are selectively expressed in the specific cortical layers [FoxP2—marker of layer VI (Ferland et al. 2003), Tbr1—marker of layer VI (Hevner et al. 2001); Etv1—marker of layer V, Rspo1—marker of layer IV, Cart—marker of layer III, Rfx3—marker of layer II (Boyle et al. 2011)]. Some of these proteins are transcription factors, which, hypothetically, could control the expression of PML.

In conclusion, our study demonstrates that PML protein is widely, but differentially, expressed in the adult brain, and suggests that PML bodies play a role in the nuclear events associated with neuronal activity.

Acknowledgments This work is supported by the grant No. 2012/05/E/NZ4/02997 from National Science Center, and by the European Regional Development Fund POIG 01.01.02-00-008/08. The authors are grateful to Dr. Tomasz Prószyński for his generous gift of immortalized fibroblasts.

References

Bernardi R, Pandolfi PP (2007) Structure, dynamics and functions of promyelocytic leukaemia nuclear bodies. Nat Rev Mol Cell Biol 8:1006–1016

Bolte S, Cordelieres FP (2006) A guided tour into subcellular colocalization analysis in light microscopy. J Microsc 224:213–232

Boyle MP, Bernard A, Thompson CL, Ng L, Boe A, Mortrud M, Hawrylycz MJ, Jones AR, Hevner RF, Lein ES (2011) Cell-type-specific consequences of Reelin deficiency in the mouse neocortex, hippocampus, and amygdala. J Comp Neurol 519:2061–2089

Butler K, Martinez LA, Tejada-Simon MV (2013) Impaired cognitive function and reduced anxiety-related behavior in a promyelocytic leukemia (PML) tumor suppressor protein-deficient mouse. Genes Brain Behav 12:189–202

Cleries R, Galvez J, Espino M, Ribes J, Nunes V, de Heredia ML (2012) BootstRatio: a web-based statistical analysis of fold-change in qPCR and RT-qPCR data using resampling methods. Comput Biol Med 42:438–445

Eskiw CH, Dellaire G, Mymryk JS, Bazett-Jones DP (2003) Size, position and dynamic behavior of PML nuclear bodies following cell stress as a paradigm for supramolecular trafficking and assembly. J Cell Sci 116:4455–4466

Eskiw CH, Dellaire G, Bazett-Jones DP (2004) Chromatin contributes to structural integrity of promyelocytic leukemia bodies through a SUMO-1-independent mechanism. J Biol Chem 279:9577–9585

Ferland RJ, Cherry TJ, Preware PO, Morrisey EE, Walsh CA (2003) Characterization of Foxp2 and Foxp1 mRNA and protein in the developing and mature brain. J Comp Neurol 460:266–279

Gambacorta M, Flenghi L, Fagioli M, Pileri S, Leoncini L, Bigerna B, Pacini R, Tanci LN, Pasqualucci L, Ascani S, Mencarelli A, Liso A, Pelicci PG, Falini B (1996) Heterogeneous nuclear expression of the promyelocytic leukemia (PML) protein in normal and neoplastic human tissues. Am J Pathol 149:2023–2035

Giorgi C, Ito K, Lin HK, Santangelo C, Wieckowski MR, Lebiedzinska M, Bononi A, Bonora M, Duszynski J, Bernardi R, Rizzuto R, Tacchetti C, Pinton P, Pandolfi PP (2010) PML regulates apoptosis at endoplasmic reticulum by modulating calcium release. Science 330:1247–1251

Guo C, Henley JM (2014) Wrestling with stress: roles of protein SUMOylation and deSUMOylation in cell stress response. IUBMB Life 66:71–77

Guo C, Hildick KL, Luo J, Dearden L, Wilkinson KA, Henley JM (2013) SENP3-mediated deSUMOylation of dynamin-related protein 1 promotes cell death following ischaemia. EMBO J 32:1514–1528

Guzzo CM, Ringel A, Cox E, Uzoma I, Zhu H, Blackshaw S, Wolberger C, Matunis MJ (2014) Characterization of the SUMO-binding activity of the myeloproliferative and mental retardation (MYM)-type zinc fingers in ZNF261 and ZNF198. PLoS One 9:e105271

Hevner RF, Shi L, Justice N, Hsueh Y, Sheng M, Smiga S, Bulfone A, Goffinet AM, Campagnoni AT, Rubenstein JL (2001) Tbr1 regulates differentiation of the preplate and layer 6. Neuron 29:353–366

Janer A, Martin E, Muriel MP, Latouche M, Fujigasaki H, Ruberg M, Brice A, Trottier Y, Sittler A (2006) PML clastosomes prevent nuclear accumulation of mutant ataxin-7 and other polyglutamine proteins. J Cell Biol 174:65–76

Koken MH, Puvion-Dutilleul F, Guillemin MC, Viron A, Linares-Cruz G, Stuurman N, de Jong L, Szostecki C, Calvo F, Chomienne C et al (1994) The t(15;17) translocation alters a nuclear body in a retinoic acid-reversible fashion. EMBO J 13:1073–1083

Koressaar T, Remm M (2007) Enhancements and modifications of primer design program Primer3. Bioinformatics 23:1289–1291

Kumada S, Uchihara T, Hayashi M, Nakamura A, Kikuchi E, Mizutani T, Oda M (2002) Promyelocytic leukemia protein is redistributed during the formation of intranuclear inclusions independent of polyglutamine expansion: an immunohistochemical study on Marinesco bodies. J Neuropathol Exp Neurol 61:984–991

Lafarga M, Berciano MT, Pena E, Mayo I, Castano JG, Bohmann D, Rodrigues JP, Tavanez JP, Carmo-Fonseca M (2002) Clastosome: a subtype of nuclear body enriched in 19S and 20S proteasomes, ubiquitin, and protein substrates of proteasome. Mol Biol Cell 13:2771–2782

Lallemand-Breitenbach V, de The H (2010) PML nuclear bodies. Cold Spring Harb Perspect Biol 2:a000661

Matsuzaki K, Minami T, Tojo M, Honda Y, Saitoh N, Nagahiro S, Saya H, Nakao M (2003) PML-nuclear bodies are involved in cellular serum response. Genes Cells 8:275–286

Michod D, Bartesaghi S, Khelifi A, Bellodi C, Berliocchi L, Nicotera P, Salomoni P (2012) Calcium-dependent dephosphorylation of the histone chaperone DAXX regulates H3.3 loading and transcription upon neuronal activation. Neuron 74:122–135

Miki T, Xu Z, Chen-Goodspeed M, Liu M, Van Oort-Jansen A, Rea MA, Zhao Z, Lee CC, Chang KS (2012) PML regulates PER2 nuclear localization and circadian function. EMBO J 31:1427–1439

Okuno H (2011) Regulation and function of immediate-early genes in the brain: beyond neuronal activity markers. Neurosci Res 69:175–186

Pawlak R, Rao BS, Melchor JP, Chattarji S, McEwen B, Strickland S (2005) Tissue plasminogen activator and plasminogen mediate stress-induced decline of neuronal and cognitive functions in the mouse hippocampus. Proc Natl Acad Sci USA 102:18201–18206

Regad T, Bellodi C, Nicotera P, Salomoni P (2009) The tumor suppressor Pml regulates cell fate in the developing neocortex. Nat Neurosci 12:132–140

Sahin U, Ferhi O, Jeanne M, Benhenda S, Berthier C, Jollivet F, Niwa-Kawakita M, Faklaris O, Setterblad N, de The H, Lallemand-Breitenbach V (2014) Oxidative stress-induced assembly of PML nuclear bodies controls sumoylation of partner proteins. J Cell Biol 204:931–945

Salomoni P (2013) The PML-Interacting Protein DAXX: histone Loading Gets into the Picture. Front Oncol 3:152

Salomoni P, Betts-Henderson J (2011) The role of PML in the nervous system. Mol Neurobiol 43:114–123

Salomoni P, Bernardi R, Bergmann S, Changou A, Tuttle S, Pandolfi PP (2005) The promyelocytic leukemia protein PML regulates c-Jun function in response to DNA damage. Blood 105:3686–3690

Untergasser A, Cutcutache I, Koressaar T, Ye J, Faircloth BC, Remm M, Rozen SG (2012) Primer3–new capabilities and interfaces. Nucleic Acids Res 40:e115

Vallian S, Gaken JA, Gingold EB, Kouzarides T, Chang KS, Farzaneh F (1998) Modulation of Fos-mediated AP-1 transcription by the promyelocytic leukemia protein. Oncogene 16:2843–2853

Villagra NT, Navascues J, Casafont I, Val-Bernal JF, Lafarga M, Berciano MT (2006) The PML-nuclear inclusion of human supraoptic neurons: a new compartment with SUMO-1- and ubiquitin-proteasome-associated domains. Neurobiol Dis 21:181–193

Walczak A, Szczepankiewicz AA, Ruszczycki B, Magalska A, Zamlynska K, Dzwonek J, Wilczek E, Zybura-Broda K, Rylski M, Malinowska M, Dabrowski M, Szczepinska T, Pawlowski K, Pyskaty M, Wlodarczyk J, Szczerbal I, Switonski M, Cremer M, Wilczynski GM (2013) Novel higher-order epigenetic regulation of the Bdnf gene upon seizures. J Neurosci 33:2507–2511

Warrell RP, de The H, Wang Z-Y, Degos L (1993) Acute promyelocytic leukemia. N Engl J Med 329:177–189

Wasiak S, Zunino R, McBride HM (2007) Bax/Bak promote sumoylation of DRP1 and its stable association with mitochondria during apoptotic cell death. J Cell Biol 177:439–450

Wilczynski GM, Konopacki FA, Wilczek E, Lasiecka Z, Gorlewicz A, Michaluk P, Wawrzyniak M, Malinowska M, Okulski P, Kolodziej LR, Konopka W, Duniec K, Mioduszewska B, Gorecki DC, Zuschratter W, Ottersen OP, Kaczmarek L (2008) Important role of matrix metalloproteinase 9 (MMP-9) in epileptogenesis. J Cell Biol 180:1021–1035

Woulfe JM, Prichett-Pejic W, Rippstein P, Munoz DG (2007) Promyelocytic leukaemia-immunoreactive neuronal intranuclear rodlets in the human brain. Neuropathol Appl Neurobiol 33:56–66

Zhong S, Muller S, Ronchetti S, Freemont PS, Dejean A, Pandolfi PP (2000) Role of SUMO-1-modified PML in nuclear body formation. Blood 95:2748–2752

Zhu J, Koken MH, Quignon F, Chelbi-Alix MK, Degos L, Wang ZY, Chen Z, de The H (1997) Arsenic-induced PML targeting onto nuclear bodies: implications for the treatment of acute promyelocytic leukemia. Proc Natl Acad Sci USA 94:3978–3983